ESRF	**Experiment title:** **Unveiling the mechanism of $Ce_{1-x}Gd_xO_{2-x/2}$ nanoparticles formation by means of in-situ combined Pair Distribution Function and Debye Function Analyses**	**Experiment number**: CH-5514
Beamline: ID15	**Date of experiment**: from: 20/10/2018 to: 23/10/2018	**Date of report**: 08/08.2022
Shifts: 9	**Local contact(s)**: CHECCHIA Stefano	*Received at ESRF:*

Names and affiliations of applicants (* indicates experimentalists):

Marco Scavini*[,1], Federica Bertolotti*[,2], Antonietta Guagliardi*[,3], Mauro Coduri*[,4], Stefano Checchia[4], Anna Bosc*[,1], Mariangela Longhi*[,1,] Masciocchi Norberto[5]

[1]Università degli Studi di Milano, Dip. di Chimica, Milano, Italy [2]Aarhus University Aarhus Institute of Advanced Study (AIAS), aarhus, Denmark, [3]CNR - Istituto di Cristallografia, Bari, Italy; [4]ESRF, [5] University of Insubria To.Sca.Lab., Como, Italy

Report

We performed an in-situ time resolved diffraction experiments to investigate the kinetics of $Ce_{1-x}Gd_xO_{2-x/2}$ nanoparticles formation, analyzing the data by means of Pair Distribution Function/Debye Function Analysis (PDF/DFA).

Brief Introduction to the scientific problem

CeO_2 and Gd-doped ceria nanoparticles have many interesting applications in different fields acting e.g. as catalysts[1] or electrocatalyst[2] for several reactions.

Nanostructuring seems to deeply affect both the defect chemistry and the transport properties of $Ce_{1-x}Gd_xO_{2-x/2}$ (hereafter CGO), improving the oxygen diffusion performance. Besides affecting the grain boundary resistivity at intermediate temperature, the crystal size is supposed to directly influence the way defects interact.[3] In CGO, Gd^{3+} and oxygen vacancies form in bulk materials large clusters with *Ia*-3 symmetry enclosed in a fluorite CeO_2-like matrix (*Fm*-3*m* symmetry).[4] The structural relaxation (distortion) of Gd^{3+} ions traps the oxygen vacancies and subtract them from the diffusion process. In a previus experiment[5] at the ID22 beamline of the ESRF we investigated the crystal structure of CGO nanoparticles with Dv≈2-3 nm prepared using a reverse micellar wet synthetic path at room temperature[6]. By PDF analysis we observed that even for very high Gd concentration (x=0.500) the Gd^{3+} relaxation process around the oxygen vacancies is completely frustrated[5] probing that the defect chemistry of nanoparticles has a completely different architecture in respect to the bulk material.

In order to comprehend the kinetics and thermodynamics of nanoparticle formation at the atomistic levelwe performed an *in-situ* diffraction study of the CGO synthesis. PDF and DFA were selected for in-situ investigation of CGO nanoparticles because, as described above and in Ref.(5), both techniques take advantage of the total scattering approach supplying complementary information. PDF analysis demonstrates its effectiveness in characterizing the structural distortions in CGO[4,5] and in identifying even small clusters of heavy metal oxides which may form during nucleation. In particular DFA can derive the size, size distribution and shape of nanoparticles unveiling also possible inhomogeneities between their surface and their core.[7]

Experimental details

0.24 M aqueous solutions with different Gd^{3+}/ Ce^{3+} ratios (=0/8, 1/7, 2/6, 3/5, 4/4) were prepared and dispersed in a mixture of n-octane, 1-butanol, and CTAB to form a micro-emulsion (ME): ME-A.

A second ME of similar composition was made using NaOH instead of Ce^{3+}/ Gd^{3+} salts: ME-B.

The two stable ME were then mixed in a flask under stirring. Mixing of the two solutions correspond to t_0. After homogenization (around 15 seconds) an aliquot of the mixed solution was syringed inside the reactor and measurements at room temperature started. Due to the procedure described above and to the ime needed for the "search procedure", measurements in general started 90 seconds after t_0.

The core of the reactor was a quartz capillary (diameter = 2 mm) mounted in a metal frame connected to two Teflon pipes for injection and overfull.

The reactor was mounted on a goniometric head on top of a rotation stage of the ID15A beamline of ESRF at 320.7 mm distance from the detector, a Dectris Pilatus 2M CdTe. Wavelength was λ = 0.182329 Å. Maximum value of momentum transfer measured was Q_{max} = 27.5 $Å^{-1}$.

During each reaction around 1000 frames, 10 sec/each were collected. Averaging blocks of 6, 30, 60 and 120 frames produced raw data with increasing signal to noise ratio but decreasing time resolution (1, 5, 10, 20 min). Using the best time resolution (1 min/pattern) we obtained good quality G(r) limiting the Q interva to Q_{max} = 22 $Å^{-1}$.

Besides, several blank solutions were prepared and measured using the same cell which are the empty cell plus solutions not changing with time varying of few components in respect to the reactive one. In particular, we collect data on the starting MEs (without mixing them) either in presence or absence of Ce and/or Gd ions. Concentration of reactants in the blank solutions is the same as in the starting solution sued for the kinetics.

For each blank about 150 frames, 10 sec/each have been collected in order to gain a larger signal to noise ratios in respect to experiments so avoiding the introduction of additional noise to the data

Results

This version of the experimental report focuses on the PDF results because DFA analysis is still in progress.

First of all, we investigated the G(r) function of the Ce and/or Gd environment in the starting solution collecting data on microemulsion ME-A and using the data set collected on n-octane, 1-butanol, and CTAB in water without rare earth ions as a background. The resulting (differential) G(r) function should be contributed mainly by the environment of Ce and/or Gd ions.

Figure 1A reported the case of pure cerium as a bue curve. Sharp peaks appear up to 10 Å suggesing that some clusterisation of Ce-containing species is present also in ME-A before strating the reaction. In the pure gadolinium case, only one sharp peak appear at ≈2.39 Å and a 2nd coordination shell is hardly visible around 3.8-4.0 Å.

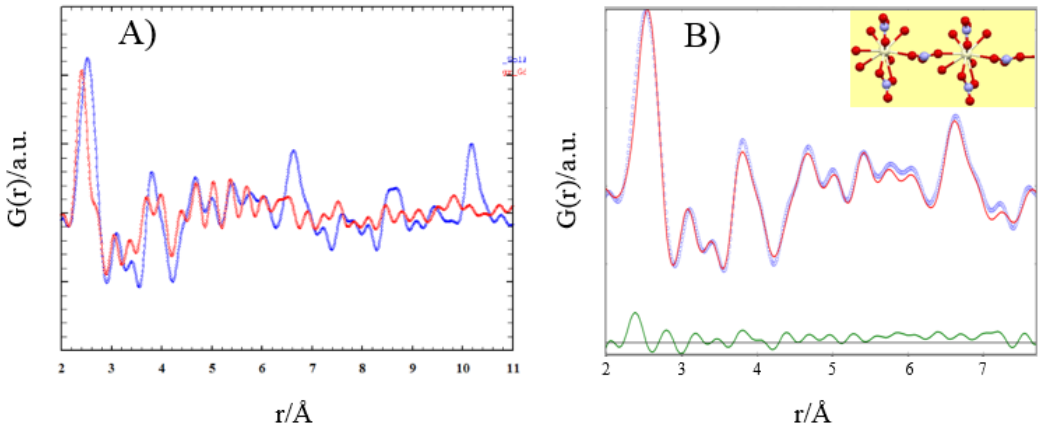

Figure 1. A) Experimental differential G(r) functions highlighting the environment of Ce (blue curve) and of Gd (red curve). See text for details. B) Fit of the blue curve of panel A with the structural model of $Ce(NO_3)_3{\cdot}4H_2O$ (red curve). Residuals are also reported as green curve. In the inset is schetched a portion of a (unrelaxed) chain of $Ce(NO_3)_3{\cdot}4H_2O$ along the c axis: White, light blue and red spheres are Ce, N and O ions, respectively. Hydrogen ions have not been considered in the model

To rationalize the G(r) in the pure cerium case, we tested different models such as fluorite-like structures with reduced dimensions (e.g. plates, roads), cerium idroxide aphases and some polimorphs of cerium nitrate. In particular, $Ce(NO_3)_3 \cdot 4H_2O$ crystallizes in *Pbca* space group; each Ce ions is coordinates by 10 oxygen ions: four of them come from H_2O molcules, four from two isolated NO_3 groups bound only to one Ce ion and the remining two from two NO_3 group, each of one is bridges two cerium ions, forming in this way chains along the crystallographic c direction.[8] Isolating one chain it is possible to obtain a reasonable fit of the experimental G(r) function, as shown in Fig.1B. Altought this model has to be improved, the fit demostrates that Ce ions form complex structures even in solution. Conversely, Gd ions seem to be sorrounded by one ordered coordination sphere.

The second step of data analysis was the investigation in-situ of the nanoparticle growth. As stated above, the first data sets were generally collected about 90 sec after the mixing of solutions A and B. This hindered to observe the initial transformation of Ce-clusters into CeO_2 nuclei.

We will discuss in some details the kinetic of pure CeO_2 synthesis.

Due to the presence of extended Ce clusters in ME-A, the choice of the background is critical.

In principle, a suitable background should contain all the contribution to scattering but that of the growing nanoparticles. However, at the very beginning of the reaction almost all the Ce ions are involved in the Ce-clusters so that the pattern of ME-A could act as background. At the end of the reaction, almost all the Ce ions should form nanoparticles, so that a suitable the background should come from ME-B. In between, we should use linear combination of the two extreems varying their weights with time, provided that adding NaOH does not change the structure of the residual Ce clusters in solution.

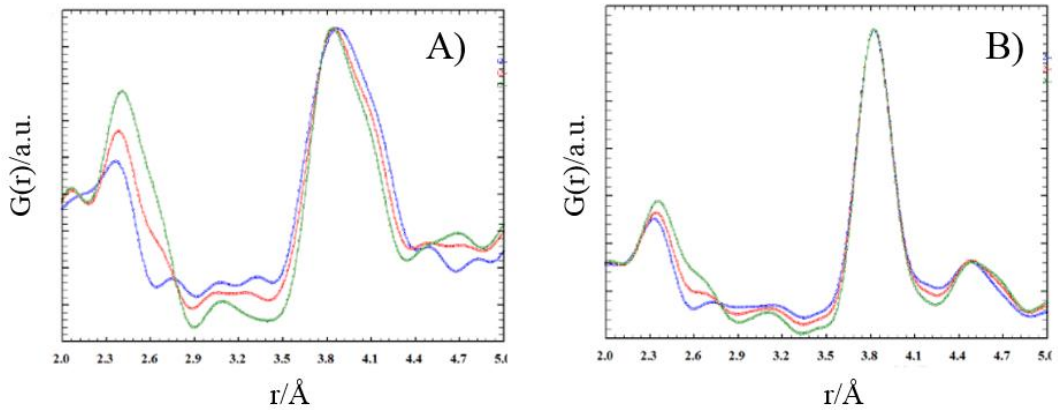

Figure 2. Low r region PDFs of CeO_2 nanoparticles at the beginning (panel A) and at the end (panel B) of the reaction using different backgrounds: solution A (blue curves), n-octane, 1-butanol, CTAB and NaOH in water (red curve) and a 1:1 linear combination of the two solutions.

In Figure 2 are reported the low *r* portion of CeO_2 nanoparticles PDFs at the beginning (panel A) and at the end (panel B) of the reaction using different backgrounds: ME-A (blue curves), ME-B (green curve) and a 1:1 linear combination of the two MEs (red curve). The background choice deeply affects the shape of the G(r) functions especially (but not only) at very short range and, as a consequence, the fit quality and results.

As additional comment, focusing on the 3.5-4.3 Å r range, correponding to the 1st Ce-Ce distance of the fluorite structure, we note that in panel A , beside the peak centered at r=3.8 Å (the tipical Ce-Ce distance in bulk CeO_2) a shoulder appears at r≈ 4.05 Å which is hardly visible in the G(r) displayed in panel B. This suggests huge atomic relaxation at the beginning of the reaction probably due to Ce^{3+} ions at the surface during CeO_2 nucleation and initial growth.

We decided to calculated experimental PDFs,using ME-B (so without Ce) as a background and fitting tha data using a two phase model formed by spherical CeO_2 fluorite nanoparticles plus $Ce(NO_3)_3 \cdot 4H_2O$, as above described. Aiming to avoid over-parametrization of the fit, we fixed all the positional degrees of freedom of the latter phase and varied only its scale factor.

In figure 3 are reported the fits of G(r) at the beginning (panels A, B) and at the end (panels C and D) of the reaction. To highligth the importance of including the $Ce(NO_3)_3 \cdot 4H_2O$ in the model, in panels A and C are reported the fits using only the CeO_2 phase and in panel B and D the best fits of the two phases model.

Including the $Ce(NO_3)_3 \cdot 4H_2O$ phase improves significantly the fit quality at the beginning of the reacion when a non negligible fraction of Ce ions is in solution. However, the biphasic fit shown in Fig.3B is far from being optimal eg. In correpondence to the 1st Ce-Ce distance (the adopted fluorite model does not allow surface relaxation) and to larger interatomic distances (e.g. in the 7-8 Å interval). Even at the end of the reaction some Ce ions are still in solution, as suggested by the calculated curves of Figs.3C and 3D.

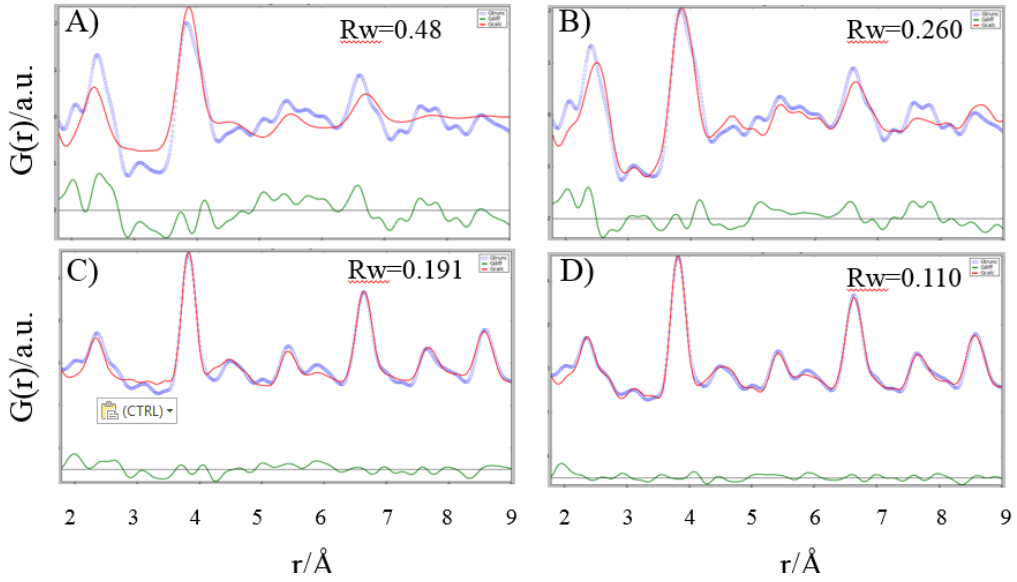

Figure 3. Blue curves depict the experimental G(r) functions of CeO_2 nanoparticles at the beginning (panels A and B) and at the end (panels C and D) of the reaction using solution B as background. In panels A and C the data have been fitted with a model with only CeO2 nanoparticles; in panels B and D aso the $Ce(NO_3)_3 \cdot 4H_2O$ is considered in the model

The fit results for the CeO_2 phase in the 2-30 Å are shown in figure 4. All the refined parameters vary rapidly at the beginning of the reaction, then the slopes are progressive reduced. For this reason we used a logarithmic scale for the abscissa values.

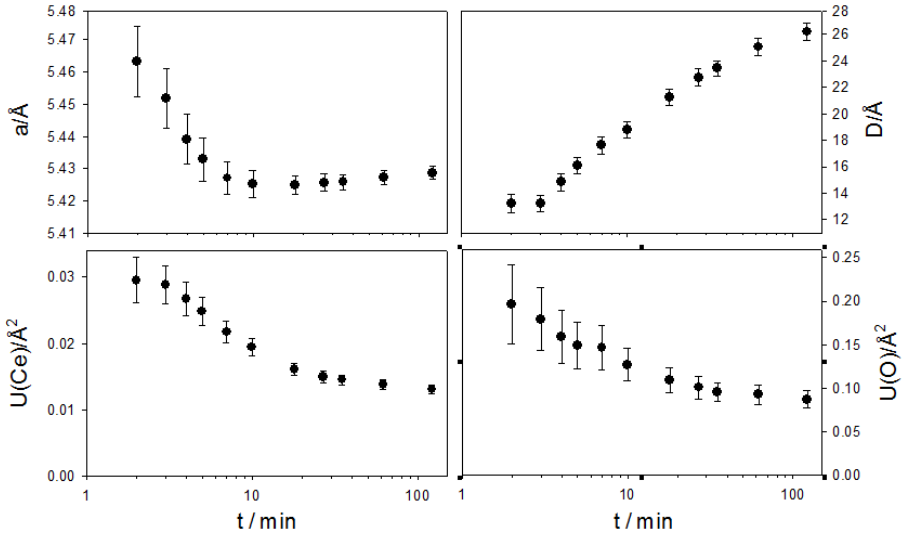

Figure 4. Fit results for the CeO_2 phase in the synthesis of CeO_2.

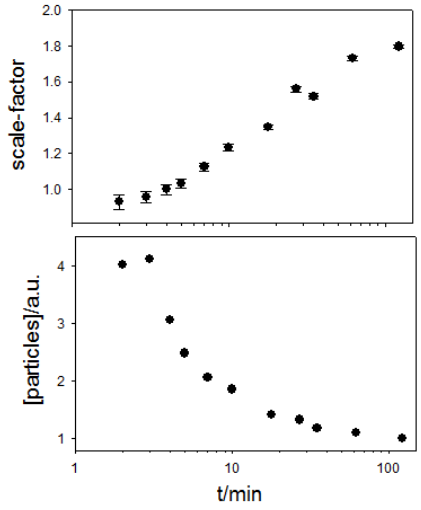

Figure 5. Up: Scale factor of CeO_2 phase. Down: concentration of particles (normalized to 1 at the end of the reaction)

During the reaction, the volume averaged particles dimensions D_V passes from ≈ 12 Å to ≈ 24 Å. At the same time, the cell constant a and the thermal parameters U(Ce) and U(O) display noticeable decreases. The trends of the U parameters point to a reduction of disorder reducing the surface-to-volume ratio. The a cell constant shrinking should be related to an incrisingly larger fraction of Ce^{4+} ions in the nanoparticles, suggesting thet Ce^{3+} are located preferentially at the surface during crystal growth.

Starting from the fitted D_V and scale factors parameters, and approximating the nanoparticles shapes to spheres of diameter D_V, we calculated the concentration of CeO_2 nanoparticles as a function of time (normalized to 1 at the largest t value). Figure 5 shows that it drops to one-quarter in respect to its initial value. The growth of final CeO_2 occur at the expence of most of the cerium oxide nuclei existing at the beginning of the reaction

Passing to the doped materials, the choice of the background is made even more complex by the additional presence of Gd^{3+} in solution. For this reason, up to now only preliminary results are shown in this experimental report. However, we note that all the different strategies tested up to now point to very similar trends of the fitted parameters, with some small differences in their absolute refined values. In Figure 6 is reported, as an example, the case of $Ce_{0.5}Gd_{0.5}O_{1.75}$ sample.

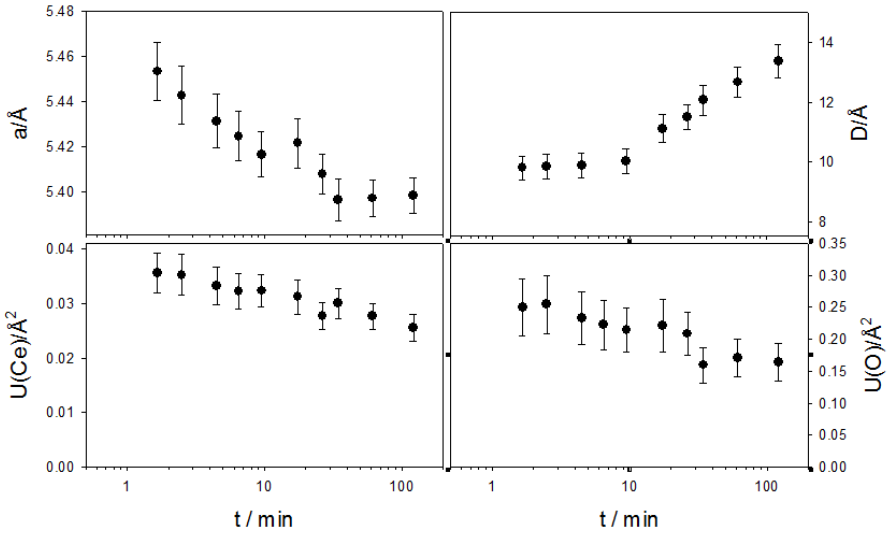

Figure 6. Fit results for the $Ce_{0.5}Gd_{0.5}O_{1.75}$ phase in the synthesis of $Ce_{0.5}Gd_{0.5}O_{1.75}$.

The fitted parameters display similar trends to the CeO_2 case. However, the particles dimension D_V is ≈ 10 Å at the beginning of the reaction, it starts increasing after an induction period of 10 minute and converges to ≈ 14 Å at the end.

We note here that a a progressive reduction of the crystal growth rate is observed on increasing the Gd concentration in the starting solutions.

The different crystal growth kinetic of pure an Gd-doped nanocrystals suggests that gadolinium inihibits in some way the crystal growth; this could originate either by the different redox properties of Ce and Gd ions, as revealed by thair Pourbaix diagram[9], or by steric mismatch due to the different ionic radii of Gd^{3+} 1.053 Å in respect to Ce^{4+} (0.97 Å) and Ce^{3+} (1.143 Å).[10]

Summary and Future Work

We performed an in-situ diffraction study of pure and Gd-doped CeO_2 nanoparticles crystal growth, analyzing the data in the real space by PDF analysis. By the experimental point of view, accurate measurements of suitable backgrounds and of MEs is mandatory for the investigations, in order to include in the calculated PDFs scattering contributions coming only (or mainly) from Ce/Gd-containing species.

Although the large majority of scattered intensities in this experiment come from the background, good quality PDFs calculated up to Q_{max} = 22 Å^{-1} were measured in one minute.

The experimental strategy allowed to follow the growth of the investigated nanomaterials in detail revealing the time evolution of the particles dimensions and of disorder. Additional data analysis approaches will be applied to extract all the pieces of structural information also with the help of ab-initio and force field simulations of nanoparticles.

In addition, also DFA data analysis is in progress to derive the shape of the growing nanoparticles quntifying also the inhomogeneities between their surface and their core, suggested by PDF analysis.

We plan to extend the present investigation to other rare earth dopants to reveal the origin of the crystal growth rate reduction of doped nanocrystals in respect to pure CeO_2. In addition, the technological importance of $Ce_{1-x}RE_xO_{2-x/2}$ materials (with RE = rare earth) make these studies interesting *per se*.

In order to detect the first instants of the reactions is mandatory to substitute our manual procedure with an automatized one. In this respect, the staff of ID15A is developing an experimental stage for liquid samples and reaction involving liquids.

References:

[1] See e. g. M. Godinho et *al*. *J Mater Sci*. **45** (2010) 593; D. N. Durgasri, *Applied Surface Science* **314** (2014) 592.

[2] N. Ai et al., Solid State Ionics **233** (2013) 87

[3] Zhi-Peng Li et *al*., *Appl. Phys. Lett*. **98** (2011) 093104

[4] M. Scavini et *al. Chem. Mater*., **24** (2012) 1338; M. Scavini et *al.*, *IUCrJ* **2** (2015) 511

[5] Experimental report of Exp. Ch5157, ID22@ESRF, 31.01-06.02.2018

[6] S. Sathyamurthy et *al*. *Nanotechnology* **16** (2005) 1960-64

[7] F. Bertolotti et *al*., *Nat. Mater*. **15** (2016) 987; A. Cervellino et al., *J. Appl. Cryst.* **48** (2015) 48, 2026; F. Bertolotti et al., *Acs Nano* **11** (2017), 3819.

[8] N. Milinski, P. RadivojevicS. Djuric, B. Ribar, 'Tetraaquatri(nitrato)cerium(III), $Ce(H_2O)_4 \cdot (NO_3)_3$, 'Crystal Structure Communications', 11 (1982) 1241-1244

[9] M. Pourbaix, Atlas d'équilibres électrochimiques, Gauthier-Villars et Cie, 1963

[10] R.D. Shannon, *Acta Cryst.* **A32** 751-767 (1976) and http://abulafia.mt.ic.ac.uk/shannon/